Asian Journal of Chemistry; Vol. 36, No. 9 (2024), 2139-2144

ASIAN JOURNAL OF CHEMISTRY

https://doi.org/10.14233/ajchem.2024.32189

Structural and Photoluminescence Characteristics of Dy^{3+} Doped Zn_2SiO_4 Phosphors for White Light Emitting Diodes

AKASH SINHA[1,*], V. JENA[1], B. VERMA[2] and KANCHAN TIWARI[2]

[1]Department of Chemistry, Government Nagarjuna P.G. College of Science, Raipur-492010, India
[2]Department of Physics, Government Nagarjuna P.G. College of Science, Raipur-492010, India

*Corresponding author: E-mail: akashsinhachem@gmail.com

Received: 26 June 2024; *Accepted*: 1 August 2024; *Published online*: 30 August 2024; AJC-21740

Silicate-based Zn_2SiO_4 phosphor was synthesized by a low-cost solid-state reaction method doped with varying concentrations of Dy^{3+} ion (1, 2, 4, 6, 8 & 10% mol). The powder X-ray diffraction results revealed that the crystal structure of the synthesized phosphor was orthorhombic, which was matched with ICCD No. 00-037-1485. The average crystallite size of Zn_2SiO_4: Dy^{3+} was determined using the Debye-Scherrer formula and the W-H plot was found to be -32 nm and -41 nm, respectively. Field emission electron microscopic study showed the surface morphology of the synthesized phosphor was irregular in shape with slight tendency of agglomeration. The photoluminescence emission spectra of the phosphor exhibited intense emission spectra at 464, 488 and 579 nm, $^4H_{15/2} \rightarrow {}^6I_{15/2}$, $^4F_{9/2} \rightarrow {}^6H_{15/2}$, $^4H_{9/2} \rightarrow {}^6H_{13/2}$ of Dy^{3+} ions, respectively when excited at 337 nm and their corresponding colour coordinates and correlated colour temperatures were also calculated.

Keywords: Solid state method, Phosphor, PXRD, Crystallite size, Photoluminescence.

INTRODUCTION

Phosphor materials are now emerging as a critical component of optoelectronic advancements in technology. The several desirable properties of these materials make them ideal for use in light-emitting diodes (LEDs) including chemical stability, long lifespan, lack of moisture sensitivity and intense colour saturation [1,2]. One of the most significant technologies of the 20th century, light-emitting diodes (LEDs) are great artificial lighting sourcesare also environmental friendly and employed in various applications such as displays, solid lasers, cathode ray tubes (CRT), plasma display panels (PDPs), field emission displays (FED), fluorescent lamps and long lifespans due to their chemical stability, high luminescence and highly saturated colour [3,4].

Phosphorus-converted white light emitting diodes or PC-WLEDs have drawn a lot of interest in the advancement of solid-state lighting technology due to their improved sustainability over traditional incandescent and fluorescent lamps [5-7]. The silicate-based inorganic phosphor shows excellent characteristics and qualities, because of their thermal stability, wide energy band gap, cheap cost, non-toxicity, multi-colour phosphorescence and great resistance towards acid, alkali and oxygen [8]. Currently, considerable efforts have been made in developing silicate-based hosts, such as $Sr_2MgSi_2O_7$ [9], $Sr_2Y_8[SiO_4]_6O_2$ [10], Ca_2SiO_4 [11], Na_2ZnSiO_4 [12], *etc.*

Usually doped phosphor materials consist of an inorganic host and rare earth (RE) ions or transition metal or a combination of both, which functions as activators and/or sensitizers. Therefore, the choice of transition metal and/or rare earth ions as a dopant is the most crucial factor during the synthesis of phosphor materials to modulate the characteristics of the host materials. The strong covalence band within silicate ions, the cations-(strong) ionic band improves chemical and thermal stability thus, most silicates become more functional when doped with rare earth elements. For example: Li_2SrSiO_4:Eu^{3+} [13], Li_2SrSiO_4:Tb^{3+} [14], Zn_2SiO_4:Eu^{3+} [15]. For generating a functional WLED, many researchers are trying to synthesize a good trivalent rare earth ion doped inorganic phosphors. Trivalent dysprosium ions (Dy^{3+}) doped phosphors have been thoroughly studied and are of great interest to many researchers because of their potential application in white light emission

[16]. As Dy^{3+} have filled 4*f* shells, well-shielded $5s^2$ and $5p^6$ orbitals and an emission transition in optical spectra that produces a sharp line, Dy^{3+} with $4f^9$ configuration has complex energy levels and different possible transitions between f levels. Sharp line spectra characterize the highly selective transitions between these f-levels. The transition from the $^4F_{9/2}$ level to the $^6H_{15/2}$ and $^6H_{13/2}$ levels respectively, produced these two emissions peaks [17]. Blue (470-500 nm) and yellow (560-600 nm) are the two main wavelength ranges in which Dy^{3+} ions radiate. The yellow to blue (Y/B) emission intensity ratio of Dy^{3+} ions must be in the right combination to produce white light emission. When classifying white light emission in the warm/cool/day area, the Y/B emission intensity ratio plays an important part. Therefore, depending on the area, Dy^{3+} may be the suitable luminescence centre to build long-lasting phosphors for white light [18]. PC-WLEDs consume less energy, have a compact design, high lifetime and brightness. Borates (*e.g.* $Ba_2LiB_5O_{10}$:Dy^{3+}) [19], aluminates (*e.g.* $MgAl_2O_4$:Dy^{3+}) [20], phosphates (*e.g.* YPO_4: Dy^{3+}) [21], silicates (*e.g.* $Sr_2MgSi_2O_{5+x}$: Dy^{3+}) [22] and molybdates (*e.g.* Y_2 $[MoO_4]_3$: Dy^{3+}) [23] are the examples of inorganic hosts in which the rare earth ions can be incorporated.

Rare earth ions doped zinc silicate is a better option than transition metal ions doped inorganic hosts for luminescence-based applications. This work reports the photoluminescence properties, colour chromaticity and potential applications of Zn_2SiO_4:Dy^{3+} phosphor for WLED. The silicate based Zn_2SiO_4:Dy^{3+} was synthesized *via* solid-state reaction technique. The structural properties of the prepared phosphor were characterized by X-ray diffraction (XRD) and scanning electron microscopy (SEM) techniques, while the chronometric characteristics (CIE) and correlated colour temperature (CCT) were investigated. The results of the photoluminescence demonstrated that the proposed phosphor had a strong emission intensity. These results revealed that the Zn_2SiO_4:Dy^{3+} is a promising near white emitting phosphor.

EXPERIMENTAL

Synthesis of phosphor: Zn_2SiO_4 phosphors doped with Dy^{3+} at varying dopant mol% were synthesized using the high temperature solid-state reaction [SSR] method. A mixture of highly pure zinc oxide (ZnO 99%), silicon dioxide (SiO_2 99%) and dysprosium oxide (Dy_2O_3 99.5%) were weighed according to their stoichiometric ratios and mixed thoroughly to obtain a homogenous powder using the agate mortar and pestle. It was allowed to sinter at 800 ºC in an air environment inside an alumina crucible for 4 h. The refined powder mixture was obtained as end product and used as such for measurements after it reached room temperature.

Characterization: The powder X-ray diffraction (P-XRD) pattern was collected using a Bruker D8 Advanced A25 Powder X-ray diffractometer and a Cu-*K*α radiation (1.5406 Å) source at 40 kV and 40 mA in the range between 10º and 80º. Surface morphologies were investigated using a high-vacuum field-emission electron microscope (FESEM) Carl Zeiss Uhr Model Gemini Sem 500 KMAT. An ATR-FTIR (Shimadzu, IR prestige 21) spectrometer was exmployed to capture the FTIR spectra between 4000 and 500 cm^{-1} at room temperature using KBr pellet method. At room temperature, the photoluminescence excitation and emission spectra were obtained using a Horiba Fluorolog Fluorescence spectrometer lifetime detector with TSCPC and spectra were collected in the 200-800 nm range.

RESULTS AND DISCUSSION

PXRD studies: The XRD data were measured using monochromatic radiation. Fig. 1 shows the PXRD patterns of pure Zn_2SiO_4 and Zn_2SiO_4:xDy^{3+} (x = 4 mol%) phosphors. It was observed that most of the position and intensity of diffraction peaks of prepared Zn_2SiO_4:Dy^{3+} phosphor was well-matched with standard XRD patterns of the rhombic structure of Zn_2SiO_4 reference card no. [ICDD: 00-037-1485]. The solid-state synthesis approach yielded micrometer particles with high crystallinity as evidenced by the strong crystalline nature observed in

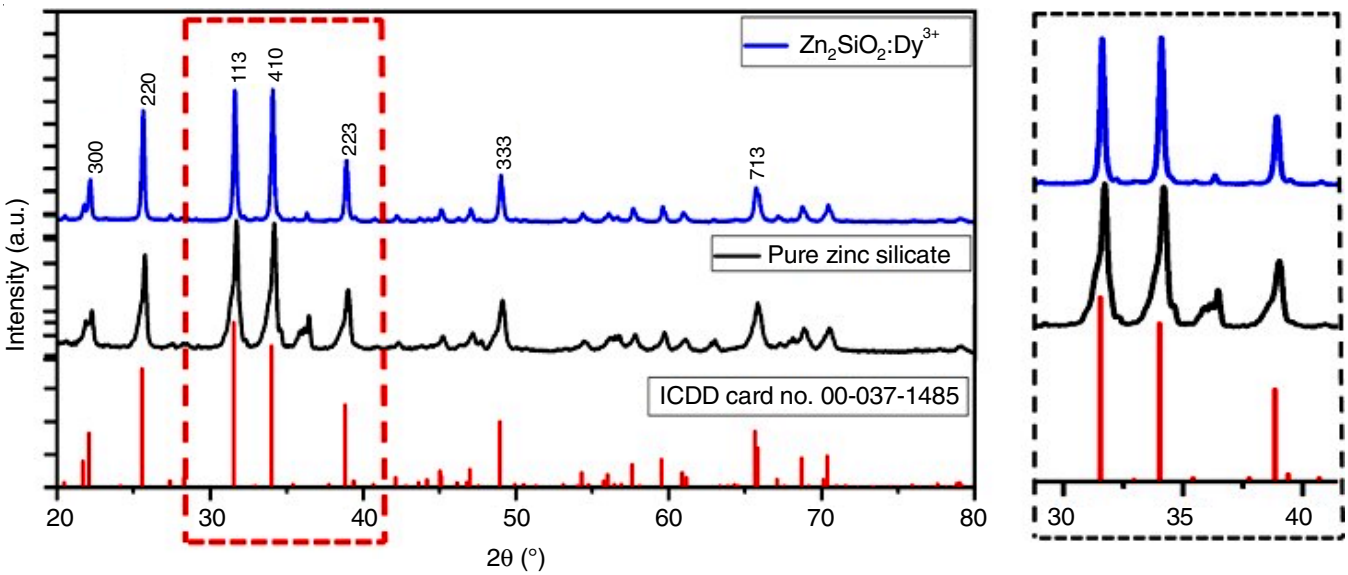

Fig. 1. PXRD pattern of pure Zn_2SiO_4 and Zn_2SiO_4:Dy^{3+} phosphor

the XRD profiles. The GSAS refinement was used for the crystal structure and the X-ray diffraction spectrum of Dy^{3+} doped Zn_2SiO_4.

Fig. 2 shows the observed that the calculated and difference XRD patterns for the refinement of Zn_2SiO_4: Dy^{3+} phosphor. The refinement factors converge to $\chi^2 = 16.54$, R_p 6.515% and R_{wp} 5.478%, respectively. The result showed the rhombohedral crystal formation and R-3 space group with the lattice parameters $a = b = 14.01$ Å, $c = 9.33$ Å, angle $\alpha = \beta = 90°$, $\gamma = 120°$ and cell volume = 1589.02 Å, Z = 18. According to the reference code no. ICDD-00-037-1485, pure Zn_2SiO_4 has lattice parameters $a = b = 13.948$ Å, $c = 9.315$ Å and cell volume = 1569.41 Å. There was contraction of lattice parameters due to Dy^{3+} incorporation into Zn_2SiO_4 lattice and hence the XRD peak shifted lightly towards lower side 2θ site. These shifts observed in the diffraction peaks may be attributed to the presence of lattice strain or lattice defects resulting from the inclusion

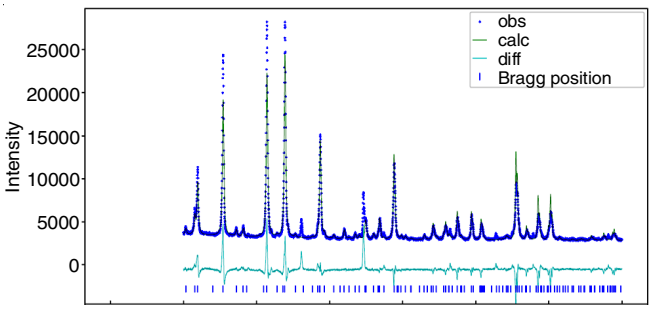

Fig. 2. Refinement graph of Zn_2SiO_4:Dy^{3+}

of a dopant. The shift of the peaks also indicated that the Zn^{2+} ions (radii = 74 pm) in the phosphors had been replaced by Dy^{3+} ions (radii = 91 pm) [24]. The ionic radii of Zn^{2+} is smaller than Dy^{3+} ion. Hence, it can easily take place of Zn ions in host lattice on doping, causing changes in unit cell parameters. The introduction of Dy^{3+} does not cause significant changes in the crystal structure of the host lattice due to small amount of doping, which illustrates the formation of similar crystal phase. Table-1 summarizes the comparative theoretical and refinement based result.

Structure measurement: The average crystallite size [D] value was calculated using the Debye-Scherrer formula:

$$D = \frac{0.9\lambda}{\beta\cos\theta} \quad (1)$$

where β is the broadening of the diffraction peak measured at half of its maximum intensity (in radians); k is the shape factor (k = 0.94); λ is wavelength of the X-ray radiation (0.154 nm for Cu-K radiation); θ is Bragg diffraction angle a Bragg angle; D is the crystallite size [24,25].

FESEM and EDX studies: Fig. 3a-b represents the morphology of the prepared Zn_2SiO_4 at different magnifications. Agglomeration, irregular and uneven size was observed on the surface of the phosphor, which might be due to heat treatment. In Fig. 4, the EDX spectrum of Zn_2SiO_4:Dy^{3+} reveals the presence of zinc, silicon and oxygen as the major elemental components, thus indicating the formation of Zn_2SiO_4 phosphors. The conformation of constituent elements like Zn [Lα at 1.012 keV

TABLE-1
STRUCTURAL PARAMETERS OF Zn_2SiO_4:Dy^{3+} PHOSPHORS TOGETHER WITH THE THEORETICAL VALUES

Phosphor	Crystallite size (nm)	Lattice constant (Å)			Angle			Cell volume (A^3)
		a (Å)	b (Å)	c (Å)	α	β	γ	
ICDD card	–	13.94	13.94	9.31	90	90	120	1569.41
Zn_2SiO_4:Dy^{3+}	32.52 nm	14.01	14.01	9.33	90	90	120	1589.02

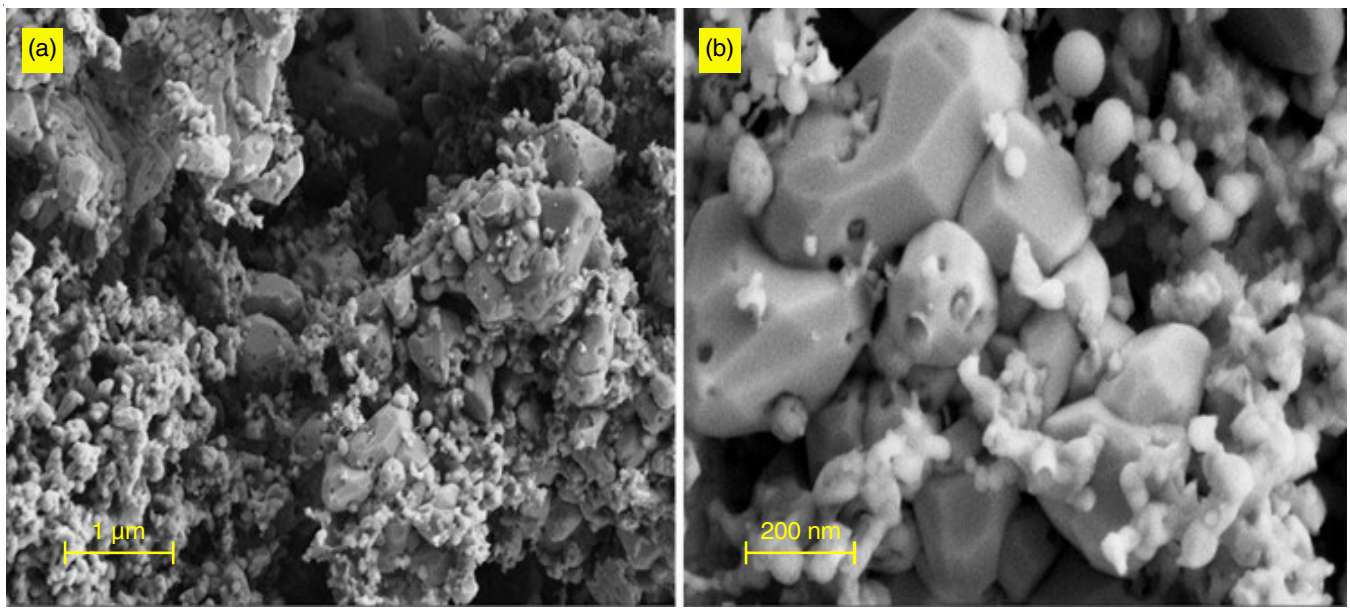

Fig. 3. FESEM images of Zn_2SiO_4:Dy^{3+} with different magnification

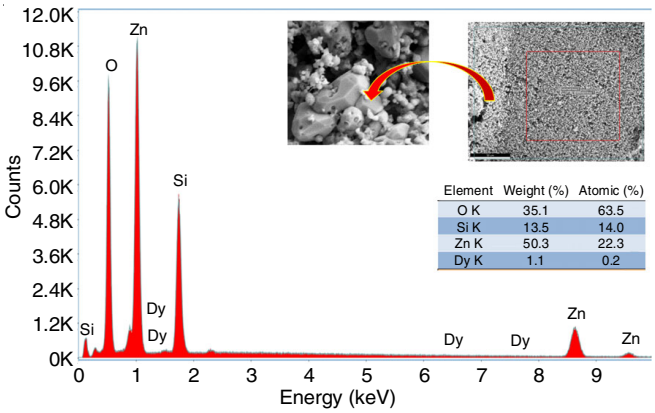

Fig. 4. EDS spectrum of Zn_2SiO_4:Dy^{3+} phosphor

and Kα at 8.637keV], Si [Kα at 1.740 keV], O [Kα at 0.525 keV] and doped Dy [Lα at 6.498 keV and Mα at 1.293 keV] that the Dy occupied a site and occupied place in a host matrix successfully.

FTIR studies: The FTIR spectrum of the prepared silicate based Zn_2SiO_4 phosphor obtained at room temperature between 500 and 4000 cm^{-1} is shown in Fig. 5. The Zn-O-Zn asymmetric vibrational mode was recognized as the band at 600 cm^{-1} whereas the Zn-O-Si symmetric stretching was detected as the band at 691 cm^{-1}. The observed band at 814 cm^{-1} showed that Si-O-Si was distorted. The asymmetric starching vibrational mode of SiO_4 was generated at 899 cm^{-1} and the stretched vibrations with a wavelength of 932 cm^{-1} were appeared in Zn-O-Si [26,27].

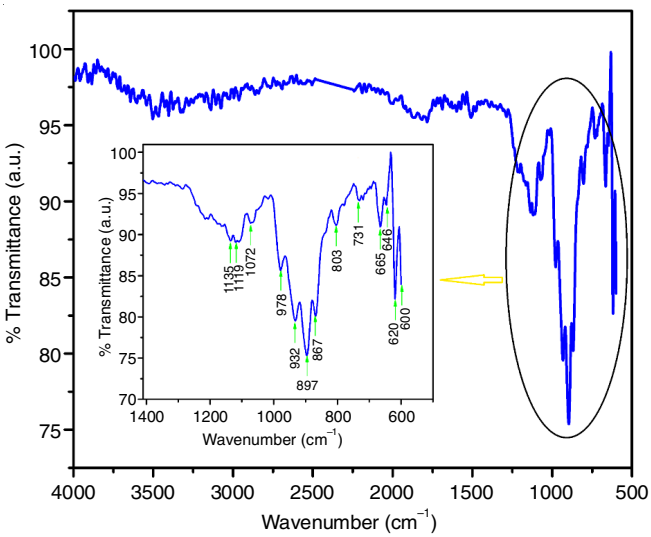

Fig. 5. FTIR spectra of Zn_2SiO_4:Dy^{3+} phosphor

Photoluminescence (PL) studies: The photoluminescence (PL) excitation spectrum of Dy^{3+} doped Zn_2SiO_4 phosphor is depicted in Fig. 6, which indicates the emission wavelength (λ_{em}) of 579 nm and obtained at room temperature range between 270 and 400 nm. The low oscillator intensity of observed peaks was caused by transitions of Dy^{3+} ions from ground energy level $^6H_{15/2}$ to higher excited energy levels, which were promoted by 4f-4f prohibited. This was the cause of all absorption peaks. The transition from $^6H_{15/2} \rightarrow {}^5F_{7/2}$ was matched by the strongest absorption line at 337 nm.

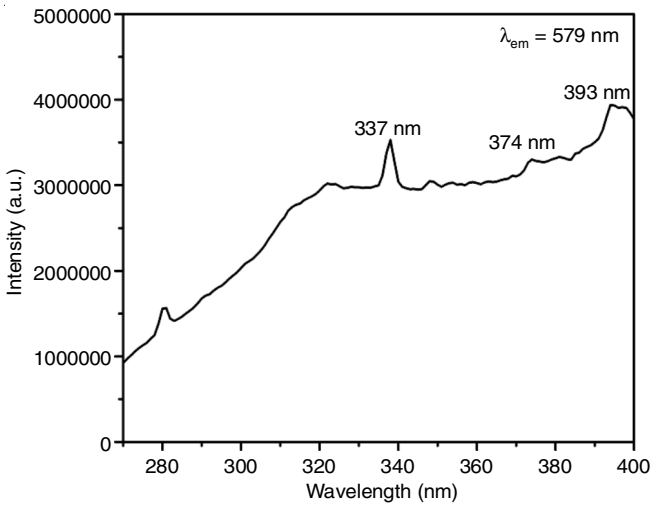

Fig. 6. PL excitation spectra of Zn_2SiO_4:Dy^3

Fig. 7 shows the PL emission spectra of Zn_2SiO_4:xDy^{3+} phosphor with various concentrations of Dy^{3+} (x = 1, 2, 4, 6, 8 and 10 mol%) were obtained at 337 nm excitation wavelength. Emission spectra from 400 nm to 750 nm have been obtained at room temperature for all mol% concentrations of Dy^{3+} doped zinc silicate. The significant emission spectra of $^4H_{15/2} \rightarrow {}^6I_{15/2}$, $^4F_{9/2} \rightarrow {}^6H_{15/2}$, $^4H_{9/2} \rightarrow {}^6H_{13/2}$ transitions of Dy^{3+} ions were seen at 464 nm, 488 nm and 579 nm respectively. All these transitions were due to f→f electronic transitions of Dy^{3+} ions. The emission spectra consisted of Dy^{3+} emission in the blue, yellow and red regions [28]. The PL emission peak for yellow emission at 579 nm ($^4H_{9/2} \rightarrow {}^6H_{13/2}$) are from the hypersensitive forced electric dipole transitions. The magnetic dipole transition was represented by 488 nm ($^4F_{9/2} \rightarrow {}^6H_{15/2}$) for blue emission [29]. The yellow emission is highly responsive to both the lattice field and crystal field environments, following the selection rule DJ = 2. As a result, the intensity of the peaks may vary depending on the specific local environment. On the other hand, the blue emission is associated with the transition of the magnetic dipole and is not affected by site symmetry; parity is allowed [30]. Thus, in present work, the blue emission is stronger than

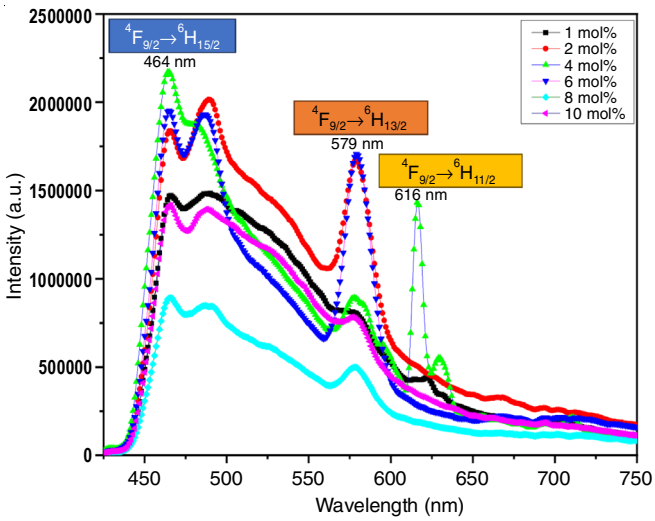

Fig. 7. PL emission spectra of Zn_2SiO_4:xDy^{3+} (x = 1, 2, 4, 6, 8 and 10 mol%)

the yellow emission, which indicates that the Dy^{3+} ions are located at high symmetry sites in host lattice. Upon the excitation wavelength 337 nm, it can be seen that the emission spectrum of the phosphors was completely different from characteristic rare earth sharp emissions but an intense broad peak appeared.

This occurred as a result of the excitation energy being provided far from the energy of the Dy^{3+}–O^{2-} charge transfer band. This demonstrated that the excitation wavelengths affect the rare-earth ion's luminescent characteristics. When the concentration of Dy^{3+} increase to 4 mol%, the emission intensity increased and when the concentration of Dy^{3+} grew further, the emission intensity dropped. This phenomenon known as concentration quenching in the host matrix, which results from a decrease in the distance between luminescent centers and creates a channel for non-radiative energy loss, is responsible for the abrupt drop in PL intensity. In addition, the radiative output of the system is reduced by this process.

The energy level diagram (Fig. 8) appears to be assigned to the $^4I_{13/2}$ energy level upon excitation of the Dy^{3+} ions to the wavelength at 337 nm and its radiative transitions like $^4H_{15/2} \rightarrow {}^6I_{15/2}$, $^4F_{9/2} \rightarrow {}^6H_{15/2}$, $^4H_{9/2} \rightarrow {}^6H_{13/2}$ energy level, the energy transfer is responsible for the exchange interaction in silicate phosphors.

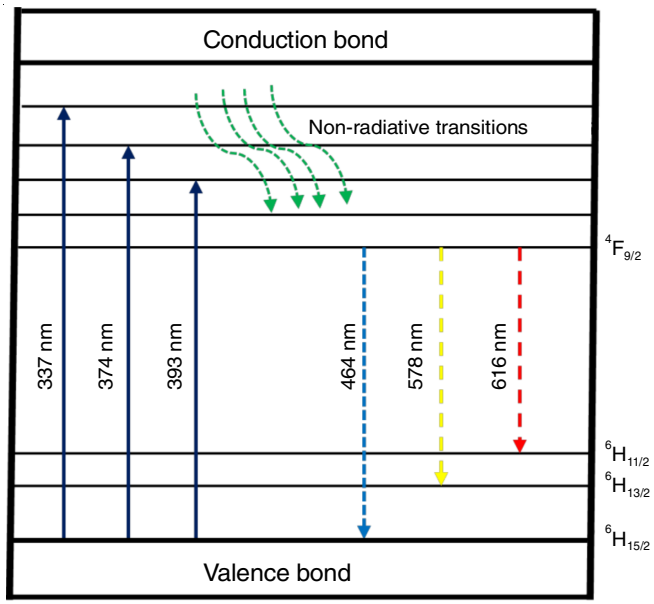

Fig. 8. Energy level diagram of Zn_2SiO_4:Dy^{3+} phosphors

Colourimetric studies: Fig. 9 presents the chromaticity diagram for the Zn_2SiO_4:4mol%Dy^{3+} phosphor as it had the optimum PL intensity. As illustrated in Fig. 7, the emission spectrum of phosphors was converted to CIE chromaticity using photoluminescence data and interactive CIE software. The white light region of the chromaticity diagram clearly shows the chromaticity coordinates (x = 0.2699, y = 0.3646) for the synthesized material Zn_2SiO_4:4mol%Dy^{3+}. The CIE coordinates in the white light region of the chromaticity diagram clearly shows that the synthesized material was lying near to the colour coordinated standard (0.3333, 0.3333) for white light emission [29]. It was observed due to the emission of $^6H_{15/2}$ [blue], $^6H_{13/2}$ [yellow] and $^6H_{11/2}$ [red] in the definite positions and intensities. The McCamy empirical equation is used to derive the colour properties of phosphor materials and the colour-correlated temperature (CCT) is a crucial parameter for assessing white light quality [31,32]. The calculated CCT value was 8064 K, which was within the cold white light zone. It is observed that the CCT for defect-assisted emission, greater than 8000 K gives cold white emission, suitable for display screens and aesthetic purposes. Considering the determined high CRI value of 73, it is apparent that the synthesized phosphor materials are ideal for white light LEDs.

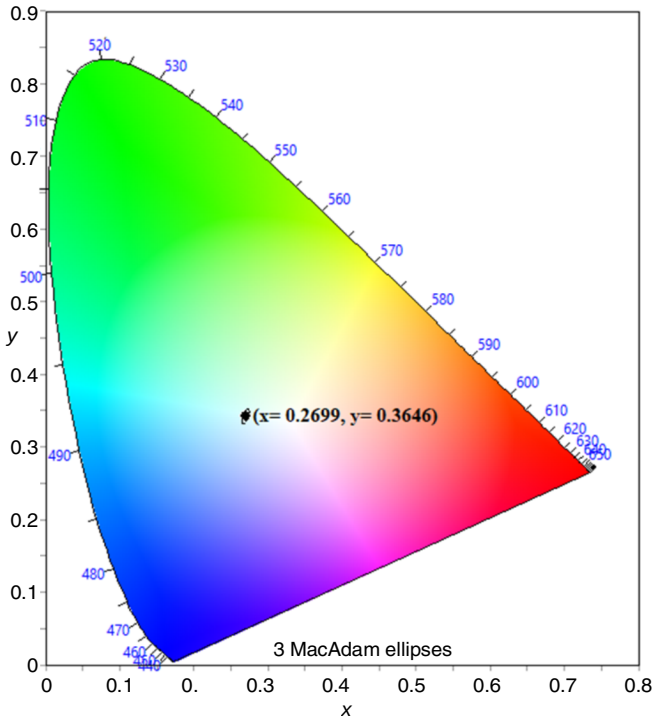

Fig. 9. CIE chromaticity diagram of synthesized Dy^{3+} doped Zn_2SiO_4 under the excitation wavelength of 337 nm and coordinates

Conclusion

In this work, we have successfully synthesized the single host Zn_2SiO_4:Dy^{3+} phosphors using conventional solid-state method at 800 ºC. The synthesis temperature is low as compared to the conventional temperature (1000-1700 ºC). The XRD results showed the crystal structure of the synthesized powder phosphors was orthorhombic which was confirmed by ICDD 00-037-1485 database. The strain occurred in the powder phosphors along with the sizes of their crystallite were calculated by both Debye Scherrer and Williamson-Hall equation from the W-H plots and found to be -32 nm and -41 nm, respectively. The refined parameters showed the variation in the lattice parameters due to doping. The relatively intense PL emission and adequate thermoluminescence glow were optimized at the doping concentration of 4 mol% Dy^{3+}. The sample doped at 4 mol% showed a white light emission according to the CIE diagram and coordinates and was found in the cold white light region. These results implied the possibility of synthesized Dy^{3+} doped zinc silicate phosphors for the possible applications in both light display devices such as WLEDs.

ACKNOWLEDGEMENTS

The authors are thankful to Indian Institute of Technology, Bhilai, India for PXRD analysis, FESEM and EDX analysis. Thanks are also due to the SAIF, MG University and NCNR, Pt. Ravishankar Shukla University, Raipur for Photoluminescence and FTIR analysis, respectively.

CONFLICT OF INTEREST

The authors declare that there is no conflict of interests regarding the publication of this article.

REFERENCES

1. K. Van den Eeckhout, P.F. Smet and D. Poelman, *Materials*, **3**, 2536 (2010); https://doi.org/10.3390/ma3042536
2. P.F. Smet, D. Poelman and M.P. Hehlen, *Opt. Mater. Expr.*, **2**, 452 (2020); https://doi.org/10.1364/OME.2.000452
3. Q. Ren, Y. Zhao, X. Wu, L. Du, M. Pei and O. Hai, *Polyhedron*, **204**, 115266 (2021); https://doi.org/10.1016/j.poly.2021.115266
4. K.-S. Sohn, B. Cho, H. Dong Park, Y. Gyu Choi and K. Hon Kim, *J. Eur. Ceram. Soc.*, **20**, 1043 (2000); https://doi.org/10.1016/S0955-2219(99)00246-0
5. L. Mishra, A. Sharma, A.K. Vishwakarma, K. Jha, M. Jayasimhadri, B.V. Ratnam, K. Jang, A.S. Rao and R.K. Sinha, *J. Lumin.*, **169**, 121 (2016); https://doi.org/10.1016/j.jlumin.2015.08.063
6. N.F. Samsudin, K.A. Matori, Z.A. Wahab, J.Y.C. Liew, Y.W. Fen, S.H.A. Aziz and M.H.M. Zaid, *Optik*, **127**, 8076 (2016); https://doi.org/10.1016/j.ijleo.2016.06.019
7. V. Sivakumar, A. Lakshmanan, S. Kalpana, R. Sangeetha Rani, R. Satheesh Kumar and M.T. Jose, *J. Lumin.*, **132**, 1917 (2012); https://doi.org/10.1016/j.jlumin.2012.03.007
8. Y. Hua and J.S. Yu, *J. Alloys Compd.*, **783**, 969 (2019); https://doi.org/10.1016/j.jallcom.2018.12.279
9. L. Babetto, S. Carlotto, A. Carlotto, M. Rancan, G. Bottaro, L. Armelao and M. Casarin, *Inorg. Chem.*, **60**, 315 (2021); https://doi.org/10.1021/acs.inorgchem.0c02956
10. Q. Zhang, X. Wang, X. Ding and Y. Wang, *Inorg. Chem.*, **56**, 6990 (2017); https://doi.org/10.1021/acs.inorgchem.7b00591
11. P. Muralimanohar, G. Srilatha, K. Sathyamoorthy, P. Vinothkumar, M. Mohapatra and P. Murugasen, *Optik*, **225**, 165807 (2021); https://doi.org/10.1016/j.ijleo.2020.165807
12. L. Cheng, X. Li, J. Sun, H. Zhong, Y. Tian, J. Wan, W. Lu, Y. Zheng, T. Yu, L. Huang, H. Yu and B. Chen, *Physica B*, **405**, 4457 (2010); https://doi.org/10.1016/j.physb.2010.08.015
13. K. Tiwari, B.G. Sharma, N. Brahme, D.P. Bisen, T. Richhariya, A. Verma, S. Sahu and A. Sinha, *Mater. Sci. Semicond. Process.*, **171**, 107997 (2024); https://doi.org/10.1016/j.mssp.2023.107997
14. K. Tiwari, B.G. Sharma, N. Brahme, D.P. Bisen, T. Richhariya, A. Verma, S. Sahu, R. Tripathi and A. Sinha, *ACS Appl. Opt. Mater.*, **2**, 433 (2024); https://doi.org/10.1021/acsaom.3c00453
15. X. Xie, J. Chen, Y. Song, X. Zhou, K. Zheng, X. Zhang, Z. Shi, H. Zou and Y. Sheng, *J. Lumin.*, **187**, 564 (2017); https://doi.org/10.1016/j.jlumin.2017.04.003
16. R. Cao, W. Shao, Y. Zhao, T. Chen, H. Ao, S. Guo, P. Liu and T. Fan, *Appl. Phys., A Mater. Sci. Process.*, **126**, 1 (2020); https://doi.org/10.1007/s00339-020-3450-7
17. S. Wang, Y. Xu, T. Chen, W. Jiang, J. Liu, X. Zhang, W. Jiang and L. Wang, *J. Alloys Compd.*, **789**, 381 (2019); https://doi.org/10.1016/j.jallcom.2019.02.229
18. M.A. Tshabalala, F.B. Dejene, S.S. Pitale, H.C. Swart and O.M. Ntwaeaborwa, *Physica B*, **439**, 126 (2014); https://doi.org/10.1016/j.physb.2013.11.022
19. V. Hegde, N. Chauhan, C.D. Viswanath, V. Kumar, K.K. Mahato and S.D. Kamath, *Solid State Sci.*, **89**, 130 (2019); https://doi.org/10.1016/j.solidstatesciences.2019.01.002
20. G. Annadurai, S.M.M. Kennedy and V. Sivakumar, *Luminescence*, **33**, 521 (2018); https://doi.org/10.1002/bio.3441
21. Y. Liu, Z. Yang, Q. Yu, X. Li, Y. Yang and P. Li, *Mater. Lett.*, **65**, 1956 (2011); https://doi.org/10.1016/j.matlet.2011.04.002
22. I. Omkaram and S. Buddhudu, *Opt. Mater.*, **32**, 8 (2009); https://doi.org/10.1016/j.optmat.2009.05.010
23. N.S. Singh, R.S. Ningthoujam, M.N. Luwang, S.D. Singh and R.K. Vatsa, *Chem. Phys. Lett.*, **480**, 237 (2009); https://doi.org/10.1016/j.cplett.2009.09.006
24. E. Chandrawanshi, D.P. Bisen, N. Brahme, G. Banjare, T. Richhariya and Y. Patle, *J. Mater. Sci. Mater. Electron.*, **31**, 14454 (2020); https://doi.org/10.1007/s10854-020-04005-2
25. Y. Tian, B. Chen, B. Tian, R. Hua, J. Sun, L. Cheng, H. Zhong, X. Li, J. Zhang, Y. Zheng, T. Yu, L. Huang and Q. Meng, *J. Alloys Compd.*, **509**, 6096 (2011); https://doi.org/10.1016/j.jallcom.2011.03.034
26. N.M. Rasdi, Y.W. Fen, R.S. Azis and N.A.S. Omar, *Optik*, **149**, 409 (2017); https://doi.org/10.1016/j.ijleo.2017.09.073
27. S.A.A. Wahab, K.A. Matori, M.H.M. Zaid, M.M. Awang Kechik, S. Hj Ab Aziz, R.A. Talib, A.Z.K. Azman, R.E.M. Khaidir, M.Z.A. Khiri and N. Effendy, *Appl. Sci.*, **10**, 4938 (2020); https://doi.org/10.3390/app10144938
28. J. Wang, J. Wang and P. Duan, *Mater. Lett.*, **107**, 96 (2013); https://doi.org/10.1016/j.matlet.2013.06.001
29. P. Mbule, D. Mlotswa, B. Mothudi and M. Dhlamini, *J. Lumin.*, **235**, 118060 (2021); https://doi.org/10.1016/j.jlumin.2021.118060
30. P.S. Mbule, B.M. Mothudi and M.S. Dhlamini, *J. Lumin.*, **192**, 853 (2017); https://doi.org/10.1016/j.jlumin.2017.08.020
31. G. Ram Banjare, D.P. Bisen, N. Brahme and C. Belodhiya, *Mater. Sci. Eng. B*, **263**, 114882 (2021); https://doi.org/10.1016/j.mseb.2020.114882
32. M. Bakr, Ü.H. Kaynar, M. Ayvacikli, S. Benourdja, Y. Karabulut, A. Hammoudeh and N. Can, *Mater. Res. Bull.*, **132**, 111010 (2020); https://doi.org/10.1016/j.materresbull.2020.111010